Wind and Structures, Vol. 1, No. 1 (1998) 1-23
DOI: http://dx.doi.org/10.12989/was.1998.1.1.001

Investigation of wind actions and effects on the Leaning Tower of Pisa

Giovanni Solari†

DISEG, Department of Structural and Geotechnical Engineering, University of Genova, Via Montallegro 1, 16145 Genova, Italy

Timothy A. Reinhold‡

Department of Civil Engineering, College of Engineering and Sciences, Clemson University, Clemson, SC 29634, U.S.A.

Flora Livesey‡†

Danish Maritime Institute, 99 Hjortekaersvej, DK-2800 Lyngby, Denmark

Abstract. This paper describes wind investigations for the Leaning Tower of Pisa which were conducted as part of an overall evaluation of its behaviour. Normally a short, stiff and heavy building would not be a candidate for detailed wind analyses. However, because of extremely high soil pressures developed from its inclination, there has been increasing concern that environmental loading such as wind actions could combine with existing conditions to cause the collapse of the tower. The studies involved wind assessment at the site as a function of wind direction, analysis of historical wind data to determine extreme wind probabilities of occurrence, estimation of structural properties, analytical and boundary layer wind tunnel investigations of wind loads and evaluation of the response with special concern for loads in the direction of inclination of the tower and significant wake effects from the neighboring cathedral for critical wind directions. The conclusions discuss the role of wind on structural safety, the precision of results attained and possible future studies involving field measurements aimed at validating or improving the analytical and boundary layer wind tunnel based assessments.

Key words: aerodynamics; dynamic response; Leaning Tower of Pisa; risk assessment; safety; statistical analysis; wind engineering; wind tunnel tests.

1. Introduction

Normally a short, stiff and heavy building such as the Leaning Tower of Pisa would not be a candidate for detailed wind engineering evaluations. However, because of extremely high soil pressures caused by its growing inclination, there has been increasing concern that environmental loading such as wind actions could combine with existing conditions to cause the collapse of the tower. The recent abrupt collapse of other Italian towers contributed to the decision to carry out wind risk

† Professor and Head
‡ Associate Professor
‡† Engineer

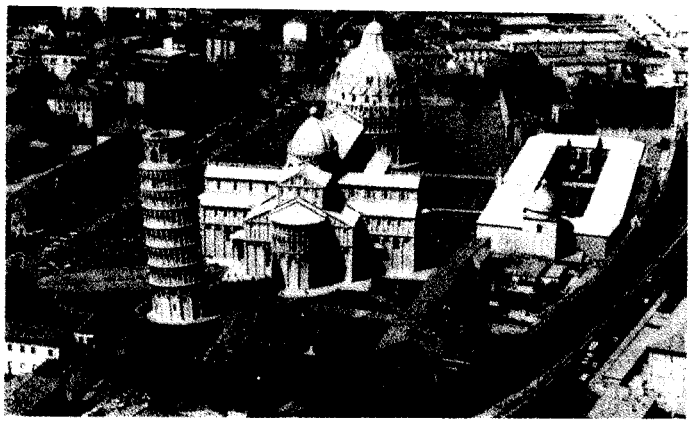

Fig. 1 View of the Piazza dei Miracoli

analyses as part of a larger coordinated effort to evaluate the overall risk posed by a variety of hazards including tilt, aging and seismic activity.

The Committee of Consolidation and Restoration Interventions on the Tower of Pisa, presided over by Professor Michele Jamiolkowski of Turin University, assigned the studies for wind actions and effects to Professor Giovanni Solari. Professor Giorgio Macchi of Pavia University, a member of the Committee, was given the scientific responsibility for the research. Boundary-layer wind tunnel tests were carried out at the Danish Maritime Institute. Ms. Flora Livesey was the project engineer involved in the tests. The testing and analysis of wind tunnel data were developed under the direction of Professor Timothy Reinhold. Prediction of the tower response and risk analyses were carried out by Professor Giovanni Solari.

The first phase of the work involved the evaluation of wind characteristics at the site as a function of wind direction, the process of historical wind data to determine extreme wind probabilities of occurrence and the analysis of the tower to estimate its structural properties. Once target wind characteristics were established, high-frequency force-balance tests were carried out in a boundary layer wind tunnel, since wake effects due to the neighboring cathedral (Fig. 1) reduced the reliability of classical analytical procedures.

In the second phase of the project, using wind tunnel model test results, some advanced analytical methods were developed and applied to determine the aerodynamic forces and the tower response. The load and response predictions for various wind velocities and directions were combined with the wind climate data to produce risk based estimates of wind effects.

This paper provides an overview of this research, pointing out the wind role on structural safety and the reliabilty of results attained. Full details on the study are reported by Solari, *et al.* (1997).

2. The Leaning Tower of Pisa

The Leaning Tower of Pisa and the other monuments standing in the Piazza dei Miracoli (Fig. 1), the cathedral and the baptistery, were erected in the Middle Ages, during the period of maximum power of Pisa. They are a manifestation of the unity between religion, civil history and culture that existed at the time. Consequently, besides their architectural and artistic value, they also serve as signs and symbols. The tower (AGI 1993, Burland and Potts 1994), begun by

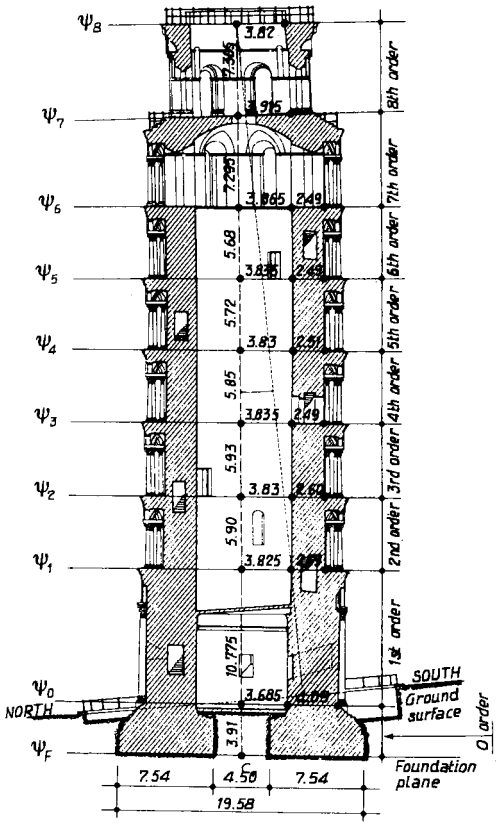

Fig. 2 Section of the tower in the plane of maximum slope

Bonanno Pisano in 1174 and finished in 1350, is the central symbol and even now is the major draw for tourism in Pisa.

The structure is composed of nine superimposed rings, termed orders, beginning with the foundation block and culminating with the bell chamber (Fig. 2). The foundation block (from the Ψ_F base plane to the Ψ_0 plane) is made of masonry cemented with San Giuliano mortar. The first order (from the Ψ_0 plane to the Ψ_1 plane) is a hollow masonry cylinder which represents a continuation of the foundation block ring. The next six orders (from the Ψ_1 plane to the Ψ_7 plane) are composed of two different structures.

The first structure is a continuation of the hollow cylinder of the first ring and is a typical example of the so called infill masonry construction. The external facing is composed of 40 cm thick San Giuliano marble. The internal facing is 30 cm thick and composed of the same marble up to the third order. It is made of soft organic limestone from the fourth to the eighth order. The infill between the two facings is made of rock fragments and stones cemented by San Giuliano mortar, with several voids of different sizes. At the seventh order there are 6 tall narrow windows with an upper arch shape.

The second structure is composed of six circular loggias, laid one upon the other, surrounding the cylinder. Each loggia is limited, on the inner side, by the external surface of the cylinder, and, on the outer side, by 30 marble equidistant columns, whose diameter diminishes upward.

The tower is capped with a bell chamber at the eighth order (from the Ψ_7 plane to the Ψ_8 top

plane). It is essentially a continuation of the lower cylinder and exhibits 6 large arched windows.

The total weight of the tower is 141,813 kN. The tilt angle is 5.5 degrees and the barycenter height above the foundation plan is 22.60 m. The weight eccentricity at the foundation plane is 2.30 m. The base overturning moment is 326,171 kNm which creates a soil pressure of 1 Mpa on the south side. As noted earlier, it is the combination of this large soil pressure with possible pressures generated by wind induced overturning moments which is of critical concern for the tower stability.

3. Wind conditions at the site

The wind climate at the tower site was evaluated using measurements of the 10 minute mean wind velocity $\overline{V}_a$ and direction $\overline{\alpha}_a$ collected every 3 hours at the meteorological station of the Military Air Force at the Pisa S. Giusto Airport. The anemometer is mounted 10 metres above ground, 6 km away from the tower. The data recorded for the period ranging from 1951 to 1991 was checked by the methods illustrated by Ballio, *et al.* (1991).

3.1. Parent population distribution

Wind velocity data was divided into nil values related to wind calm conditions and non nil velocity values. Non nil values were further divided into m=12 sub-data bases, the j-th of which comprises the velocity values associated with the j-th sector of wind direction (j = 1,2,..m). This sector is 30° wide and centered around the $\alpha_j=(2j\text{-}1)\times 15°$ angle, α=0° being the direction of the wind coming from the north.

The probability that the wind blows from the j-th sector with velocity $V=\overline{V}_a\neq 0$ is given by:

$$f_{Vj}(v)=A_j\, f_{Vj}^2(v) \quad (v>0;\ j=1,2,...m) \tag{1}$$

where A_j is the probability, conditioned to V>0, that the wind blows from the j-th sector (A_1+..+ A_m=1); v is the state variable of V; $f_{Vj}^S(v)$ is the probability density function (*pdf*) of the mean wind velocity coming from the j-th sector (Weibull 1951):

$$f_{Vj}^S(v)=\frac{k_j}{c_j}\left(\frac{v}{c_j}\right)^{k_j-1}\exp\left[-\left(\frac{v}{c_j}\right)^{k_j}\right] \quad (v>0;\ j=1,2,\cdots m) \tag{2}$$

k_j, c_j being the model parameters. The *pdf* of the parent population is given by (Solari 1996a):

$$f_V(v)=P_o\,\delta(v)+(1-P_o)\sum_1^m j\,A_j\,\frac{k_j}{c_j}\left(\frac{v}{c_j}\right)^{k_j-1}\exp\left[-\left(\frac{v}{c_j}\right)^{k_j}\right] \quad (v\geq 0) \tag{3}$$

where $\delta(.)$ is the Dirac operator and P_o is the probability that V=0.

Referring to Solari, *et al.* (1997) for a full description of this procedure and other statistical methods, Fig. 3 shows the polar joint distribution of $\overline{V}_a$, $\overline{\alpha}_a$. Each point along the innermost contour represents the wind speed exceeded on average 1% of the time, within a 30° sector centered on that direction. Other contours correspond to probability levels of 0.1%, 0.01%, 0.001%, 0.0001%. The most frequent winds come from east-north-east and from west-south-west. The strongest winds have no preferential direction, except for the reduced wind speeds from north-

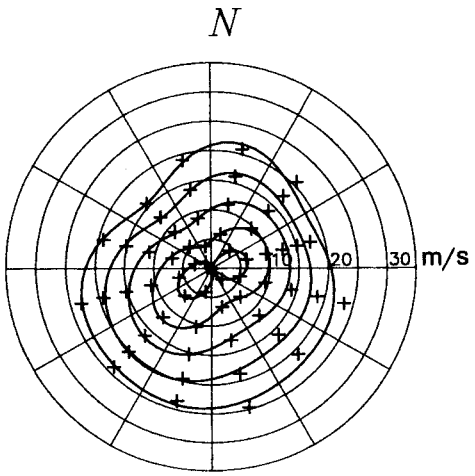

Fig. 3 Joint distribution of $\overline{V}_a$, $\overline{\alpha}_a$

west.

3.2. Distribution of extreme winds

The cumulative distribution function (*cdf*) F_M of the yearly maximum value of $V=\overline{V}_a$ was determined by several methods (Solari 1996b, Solari, *et al.* 1997), two of which are described below.

The first method applies the asymptotic type I distribution (Gumbel 1958) to the first three yearly maxima of $\overline{V}_a$:

$$F_M(v) = \exp\{-\exp[-a(v-u)]\} \tag{4}$$

Using the resistant method (Hoaglin, *et al.* 1983), a=0.459 s/m, u=15.905 m/s.

The second procedure represents the wind speed as a stochastic stationary process (Davenport 1968, Gomes and Vickery 1977):

$$F_M(v) = \exp[-\lambda f_V(v)] \tag{5}$$

where f_V is the *pdf* of the parent population (Eq. (3)) and λ=5328 m/s is the model parameter estimated by counting the threshold up-crossings.

Results of the extreme wind velocity analyses are shown in Fig. 4 where $\overline{R}=1/[1-F_M(v)]$ is the mean return period. The crosses correspond to the order statistics of the first 3 yearly maxima of $\overline{V}_a$. Since k_j parameters in Eq. (3) are greater than one, the asymptotic distribution produces conservative estimates of wind speeds at large return periods (Lagomarsino, *et al.* 1992).

3.3. Target wind characteristics for the model study

A detailed model of buildings within a 600 m radius from the tower was constructed. Consequently, wind characteristics at the 600 m radius were selected as the target reference wind conditions for the wind tunnel study. Furthermore, the mean wind velocity and direction at the 600 m radius and a height of 100 m were chosen as the reference wind velocity $\overline{V}_r$ and the reference wind direction $\overline{\alpha}_r$.

The study of the reference wind, i.e., the wind not disturbed by the cathedral, the baptistery,

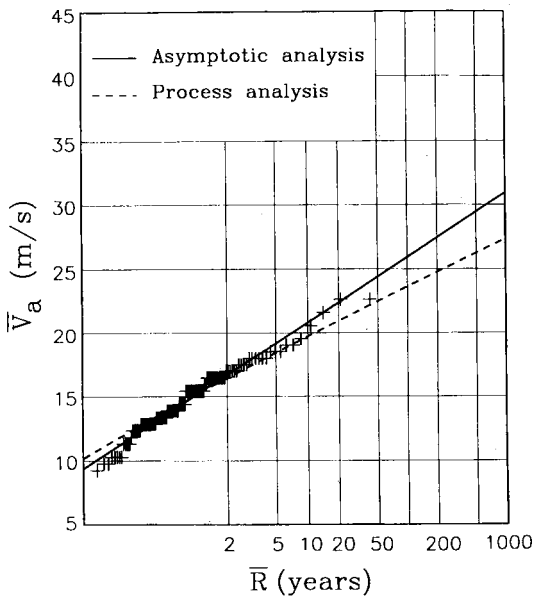

Fig. 4 Distribution of the yearly maximum value of $\overline{V}_a$

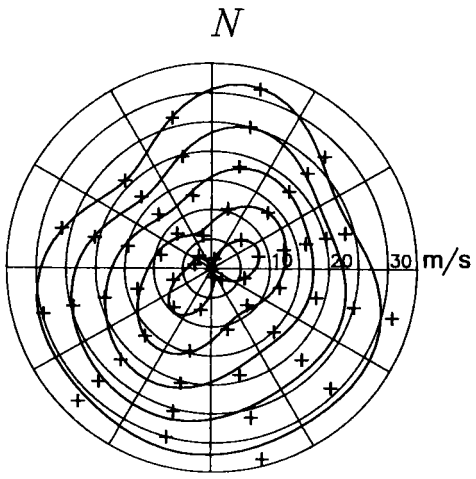

Fig. 5 Joint distribution of $\overline{V}_r$, $\overline{\alpha}_r$

the boundary wall and the tower itself, was carried out with the hypothesis of a neutral atmosphere, using a detailed representation of the surface roughness around the tower and the airport (Solari, *et al.* 1997). Airport measurements, $\overline{V}_a$, $\overline{\alpha}_a$, were transformed in reference wind values, $\overline{V}_r$, $\overline{\alpha}_r$, by a mixed approach based on the computer program A9232 (ESDU 1992) and a method stated by Zilitinkevich (1989).

The results demonstrated that the wind characteristics at the anemometer are almost independent of wind direction and may be schematized by a flow in equilibrium over a homogeneous terrain with a roughness length $(z_o)_a$=0.05 m. The reference wind field may be schematized by 3 classes of exposure, A,B,C, in equilibrium over 3 different homogeneous terrains with roughness lengths $(z_o)_A$=0.68 m (for α_r ranging from 0° to 210°, $(z_o)_B$=0.48 m (for α_r ranging

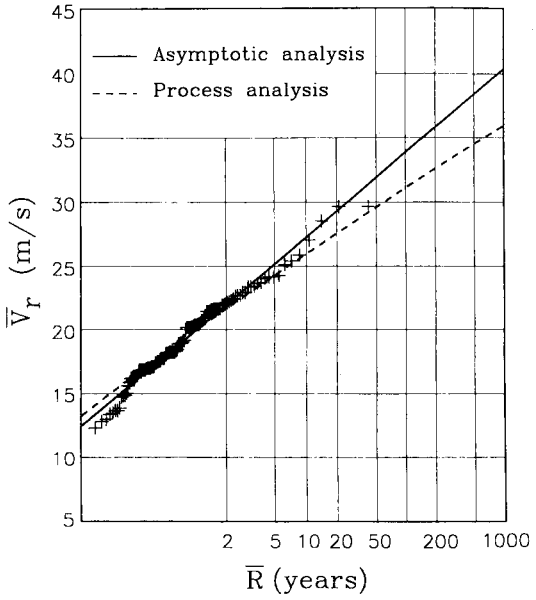

Fig. 6 Distribution of the yearly maximum value of $\overline{V}_r$

from 210° to 300° and from 330° to 360°), $(z_o)_C$=0.07 m (for $\overline{\alpha}_r$ ranging from 300° to 330°).

Setting $V=\overline{V}_r$, the new data base was submitted to the same probabilistic analyses already described in sections 3.1 and 3.2. Fig. 5 (analogous to Fig. 3) illustrates the joint distribution of $\overline{V}_r$, $\overline{\alpha}_r$. Fig. 6 (analogous to Fig. 4) shows the distributions of the yearly maximum values of $\overline{V}_r$, where a=0.355 s/m, u=20.916 m/s; λ=5906 m/s.

From a qualitative viewpoint, the results associated with $\overline{V}_r$, $\overline{\alpha}_r$ exhibit analogous properties to the results referred to $\overline{V}_a$, $\overline{\alpha}_a$. From a quantitative viewpoint, the mean velocity at 100 m height, although related to a rougher terrain, is higher than the 10 m mean velocity at the airport.

4. Boundary-layer wind tunnel tests

Model tests on the tower were carried out at a scale of 1:200 in the 2.6 m wide boundary-layer wind tunnel at the Danish Maritime Institute (DMI).

4.1. Model description

A rigid foam model of the tower (Fig. 7) was constructed for mounting on two high-frequency force balances.

The first balance was a 5-component cantilevered beam type with gauges mounted at two levels on a central post. The gauges were configured to allow overturning moments in two orthogonal directions to be measured at two heights. The lower height corresponded to the base of the tower so that the bottom set of gauges measured the base overturning moment. Shear forces were determined from the difference in the overturning moments at the two levels divided by the vertical distance between the two sets of gauges. Torsion was not of interest, so was not monitored.

The second balance was a very sensitive, very stiff 2-component balance with a natural fre-

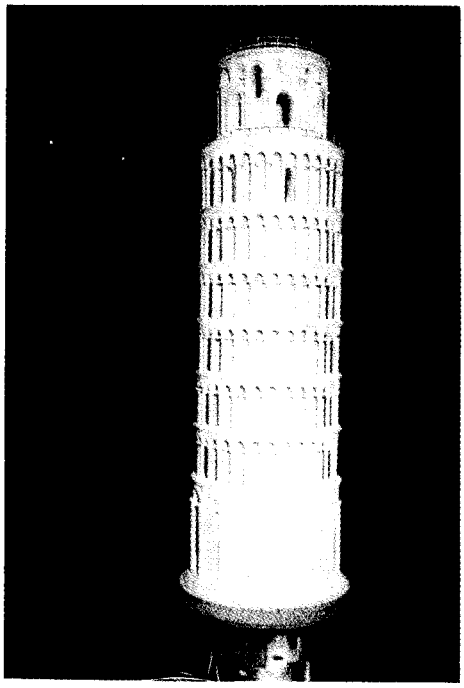

Fig. 7 Photograph of the model of the Tower of Pisa

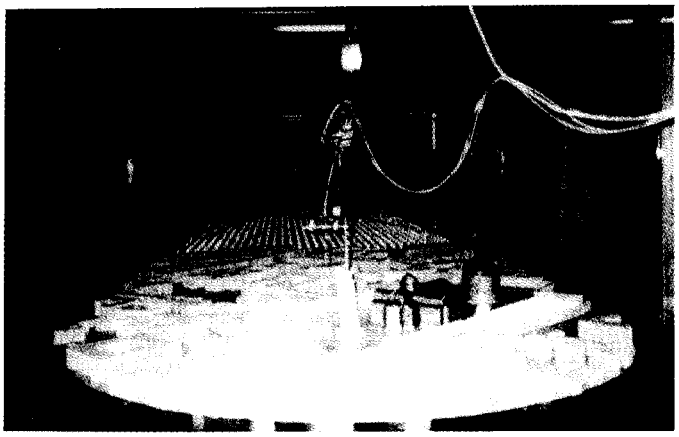

Fig. 8 Photograph of a selected portion of the proximity model mounted in the wind tunnel

quency of approximately 200 Hz and about 5 times the sensitivity of the 5-component balance. The 5-component balance was mounted on the 2-component balance and oriented in the wind tunnel to compare the alongwind forces and moments measured by the two devices (i.e., the most relevant loads for the stability of the structure).

Buildings surrounding the tower within a 600 m radius were located on a flexible plastic mat with a diameter of 6 m. The greatest attention was given to modelling structures within 250 m of the tower; this portion of the model fit on the 2.5 m diameter turntable of the tunnel. The remainder of the model was cut into pie-shaped pieces to allow placement of the appropriate parts upwind of the tower for different wind directions. Fig. 8 shows a selected portion of this model.

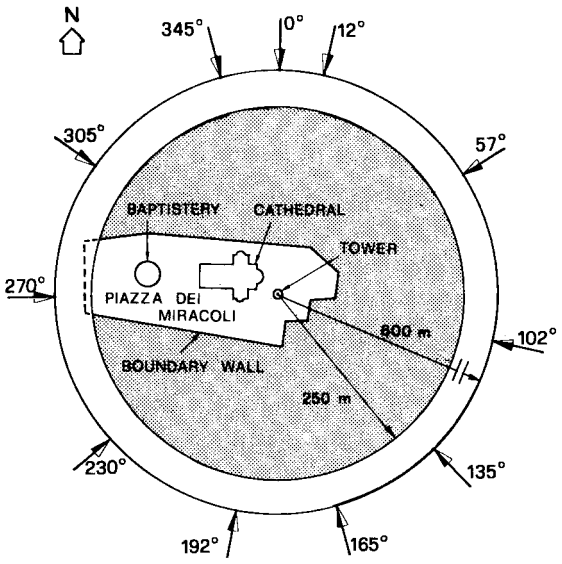

Fig. 9 Arrangement of wind tunnel tests

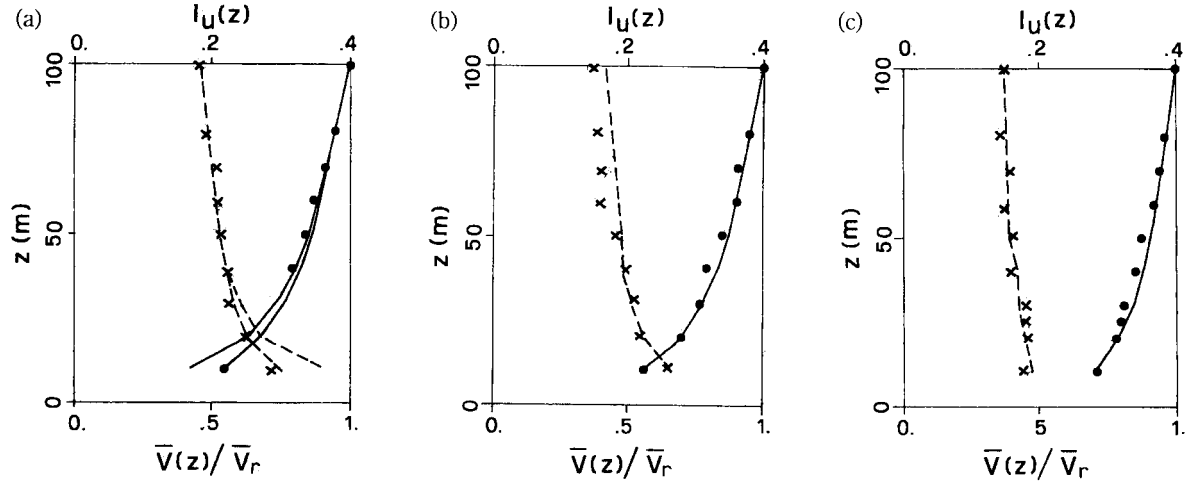

Fig. 10 Comparison of target and simulated mean wind profiles (solid lines, dots) and turbulence intensities (dashed lines, crosses): (a) class of exposure *A* (z_o=0.68 m); (b) class of exposure *B* (z_o=0.48 m); (c) class of exposure *C* (z_o=0.07 m)

4.2. Wind velocity

Wind tunnel tests were carried out for 11 different directions of the oncoming reference wind ($\overline{\alpha}_r$=0°, 12°, 57°, 102°, 135°, 165°, 192°, 230°, 270°, 305°, 345°) (Fig. 9). Three different velocity profiles were simulated 600 m upstream of the tower. These profiles provided the best fitting to the target reference wind conditions. Target profiles were achieved using a combination of spires at the entrance of the test section and a length of floor roughness. Trip boards were also used at the base of the spires to increase the boundary-layer development and the turbulence throughout the entire boundary-layer depth. Mean wind velocities $\overline{V}(z)$ and longitudinal turbulence intensities $I_u(z)$ were measured by a pitot tube and a hot-film anemometer. Fig. 10

shows the profiles given from these series of tests which most closely match the target profiles. Dots and crosses represent measured values while lines represent target values or their ranges.

4.3. Force balance tests

Force balance tests were conducted at the 11 selected wind directions. Mean values were measured for a sampling time of 60 s with zero wind checks both before and after the tests to ensure reliability of the data. Dynamic loads were measured at wind velocities of approximately 6 and 12 m/s, with the time series recorded for 180 s. These records were subsequently analysed to determine the power spectral density function (*psdf*) of the various force and moment components.

The model was initially excited with a series of impulse loads in order to obtain decaying time histories from which the mechanical admittance of the model was derived. Resonance response of the model was removed by dividing the measured *psdf* by the mechanical admittance.

Let *x,y,z* be a local Cartesian reference system with the origin at *O; z* is vertical and directed upwards, *x* is aligned with the oncoming flow, *O* lies on the floor of the tunnel. Mean and root-mean-square (*rms*) values of the shear forces and overturning moments were given in terms of non-dimensional coefficients defined by:

$$\bar{C}_{M\alpha}=\frac{2\bar{M}_{1\alpha}}{\rho\bar{V}_r^2 bh^2};\ \bar{C}_{T\alpha}=\frac{2\bar{T}_{1\alpha}}{\rho\bar{V}_r^2 bh}\quad(\alpha=x,y) \tag{6}$$

$$C'_{M\alpha}=\frac{2M'_{1\alpha}}{\rho\bar{V}_r^2 bh^2};\ C'_{T\alpha}=\frac{2T'_{1\alpha}}{\rho\bar{V}_r^2 bh}\quad(\alpha=x,y) \tag{7}$$

where $\bar{M}_{1x}$, $\bar{M}_{1y}$ are the mean components of the base overturning moment around the *x,y* axes; $\bar{T}_{1x}$, $\bar{T}_{1y}$ are the mean values of the *x,y* components of the base shear force; M'_{1x}, M'_{1y} are the *rms* components of the base overturning moment around the *x, y* axes; T'_{1x}, T'_{1y} are the *rms x, y* components of the shear force at the base; $\rho=1.22$ kg/m^3 is the air density; b=16 m and h=50 m are the reference full-scale width and height of the tower.

Table 1 gives a list of the base reaction coefficients furnished by the 5-component balance, in-

Table 1 Base reaction coefficients

$\alpha_r(^o)$	$\bar{C}_{Mx}$	$\bar{C}_{My}$	$\bar{C}_{Tx}$	$\bar{C}_{Ty}$	C'_{Mx}	C'_{My}	C'_{Tx}	C'_{Ty}	$\tilde{C}'_{Mx}$	$\tilde{C}'_{My}$
0	0.00	0.32	0.52	-0.04	0.198	0.198	0.273	0.248	0.053	0.104
12	0.01	0.31	0.50	-0.04	0.211	0.187	0.258	0.267	0.055	0.106
57	0.03	0.24	0.37	-0.06	0.193	0.166	0.227	0.250	0.050	0.107
102	0.01	0.22	0.33	-0.04	0.151	0.166	0.226	0.191	0.049	0.092
135	0.00	0.24	0.34	-0.02	0.158	0.158	0.221	0.201	0.051	0.092
165	-0.02	0.30	0.44	0.04	0.154	0.154	0.221	0.213	0.054	0.104
192	-0.03	0.27	0.41	0.06	0.187	0.148	0.211	0.214	0.053	0.101
230	-0.01	0.26	0.41	0.03	0.162	0.181	0.237	0.190	0.048	0.084
270	0.03	0.24	0.34	-0.09	0.192	0.188	0.245	0.238	0.048	0.081
305	-0.01	0.08	0.08	0.02	0.156	0.175	0.225	0.192	0.051	0.057
345	-0.01	0.31	0.49	0.00	0.209	0.218	0.301	0.265	0.048	0.100

cluding the rms overturning moment coefficients $\widetilde{C}'_{M\alpha}$ with resonance removed. The agreement of these results with those provided by the 2-component balance was verified (Solari, *et al.* 1997).

All wind tunnel tests were carried out varying the mean wind velocity to ascertain that the results were independent of the Reynolds number.

5. Structural modelling

The natural frequencies, normal modes and modal damping coefficients of the Tower of Pisa were calculated by means of a finite element model (Fig. 11) composed of superimposed beam elements with 6 degrees of freedom per node. The model comprises 18 nodes and 17 elements. It is referred to the same Cartesian system previously used for the wind tunnel tests.

In conformity with the schemes used by Faccioli and Grandori (1994), the geometrical properties of the elements were evaluated idealizing each order of the tower by a hollow cylinder, neglecting the contribution of external loggias. The areas and the moments of inertia of the cross-sections (A,J) were calculated by making the sections homogeneous with reference to the mean value 0.8×10^{11} N/m^2 of the elastic modulus of the San Giuliano marble. It was moreover assumed that the elastic modulus of the infill masonry is 0.625×10^{10} N/m^2. The shear areas were conventionally determined by dividing the cross-sectional areas by 1.3. Without specific data, the Poisson coefficient of the masonry structure was set equal to 0.2. The masses of the tower were uniformly distributed over the elements (μ). The mass moments of inertia (I) were concentrated in the nodes.

Soil flexibility was reproduced by the assemblage of the stiffness matrix of the unrestrained

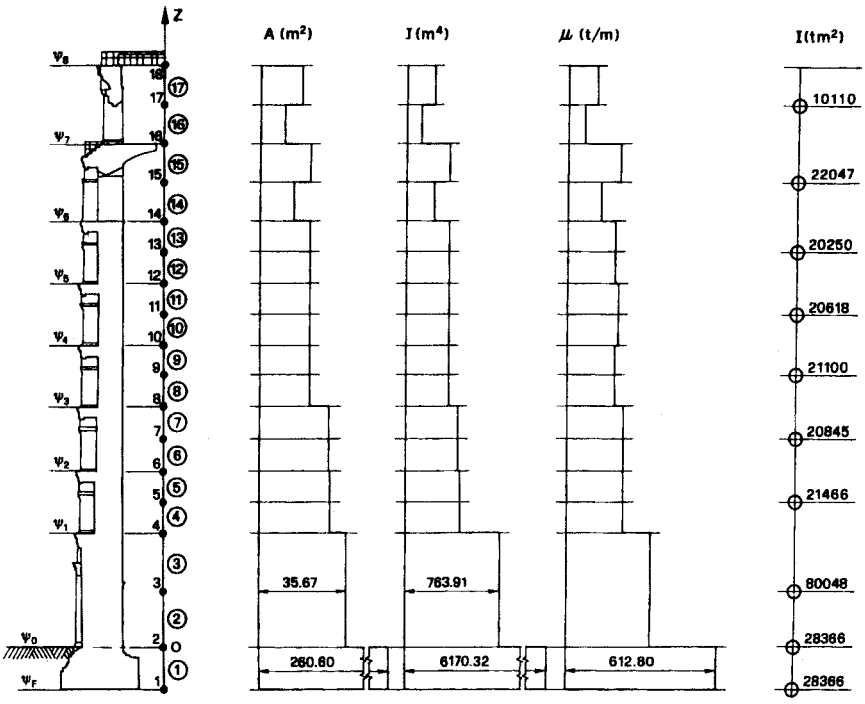

Fig. 11 Finite element model and structural parameters

Table 2 Natural frequencies and damping coefficients

k	n_k(Hz)	ξ_k
1,2	0.703	0.035
3,4	3.306	0.200
5,6	10.649	0.100
7,8	22.712	0.070
9,12	36.895	0.050
11,12	49.355	0.050

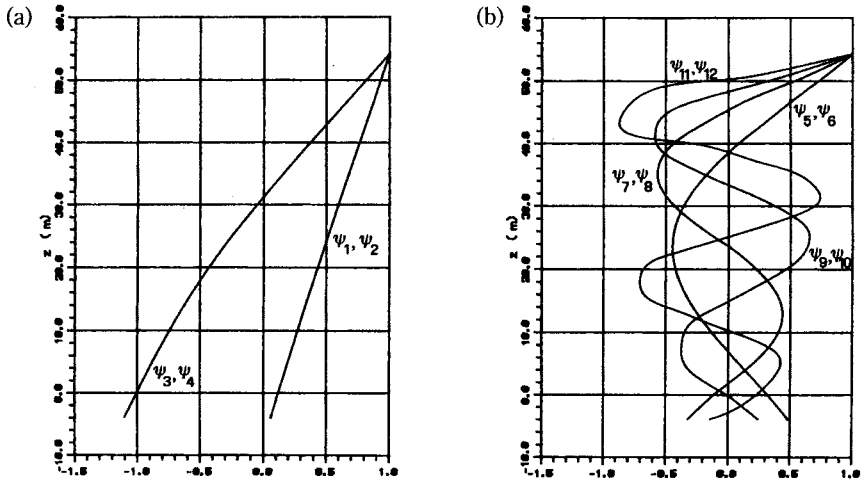

Fig. 12 Flexural modes: (a) soil-structure interaction modes; (b) masonry modes

model with the stiffness matrix of the soil-foundation system calculated by Faccioli and Grandori (1994) schematizing the soil through different models. The damping properties of the soil-foundation-structure system were evaluated by the method proposed by Solari and Stura (1979), assuming a 5% damping coefficient of the masonry structure and a 3% histeretic soil damping. Table 2 lists the natural frequencies n_k and the damping coefficients ξ_k (k=1,2,..12) of the tower. Fig. 12 shows the related mode shapes ψ_k (z) normalized at a top unit displacement. The axial and the torsional modes were considered as uninfluential with regard to the dynamic response of the tower to the wind action.

The first two pairs of normal modes (Fig. 12a) are classic soil-structure interaction mode shapes. With reference to the former modes, the tower exhibits a rigid rocking motion around its base and a low soil energy dissipation of the prevailing histeretic type. With reference to the latter modes, the tower is subjected to rigid swaying and rocking mixed motions producing a large amount of soil radiation damping. The upper modes (Fig. 12b) involve displacements and energy dissipations increasingly localized in the masonry part of the structure.

It is interesting to observe that, due to its constraint at the base, the Tower of Pisa has a fundamental frequency which is typical of tall, light and flexible buildings.

6. Aerodynamic forces

The actions applied by the wind on the Tower of Pisa were derived from the results of the boundary-layer wind tunnel force balance tests using an aerodynamic model consisting of 8 ele-

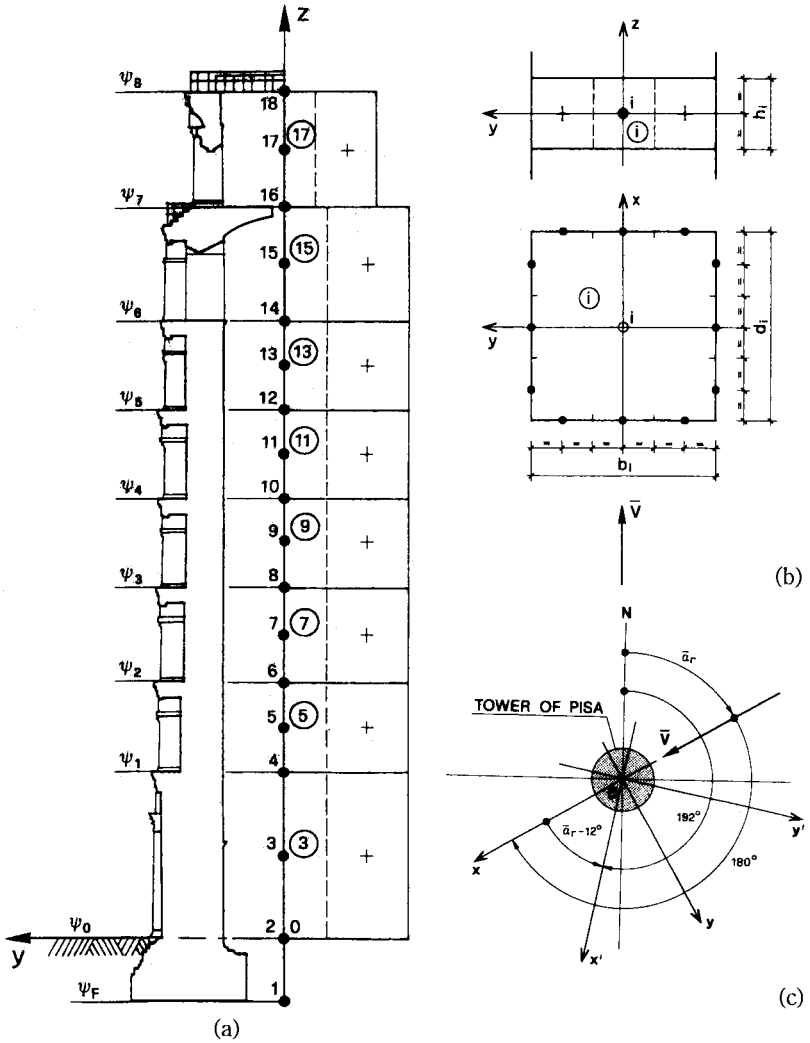

Fig. 13 Aerodynamic model of the Tower of Pisa

ments (Fig. 13a). Each element corresponds to one of the 8 orders of the tower above the ground. The external surface of each element consists of 4 faces, 2 by 2 parallel to the x,y axes ($b_3=d_3=..=b_{15}=d_{15}=16$ m; $b_{17}=d_{17}=12$ m); each face is further divided into 3 homogeneous screens (Fig. 13b). Fig. 13(c) shows the reference system; the x axis, parallel to the $\bar{\alpha}_r$ reference direction, is rotated clockwise $180°+\bar{\alpha}_r$ with respect to the north; the x' axis, aligned with the direction of maximum slope, is rotated 192° with respect to the north, $\bar{\alpha}_r - 12°$ with respect to x.

The aerodynamic forces were first applied in the centers of the above $8\times4\times3$ screens, then idealized (Solari 1985) as a system of alongwind and acrosswind forces, F_{xi}, F_{yi}, concentrated in the nodes of the structural model coinciding with the centers of the elements of the aerodynamic model:

$$F_{\alpha i} = \bar{F}_{\alpha i} + f_{\alpha i} \quad (\alpha = x,y;\ i = 3,5,\cdots 17) \tag{8}$$

where $\bar{F}_{\alpha i}$ is the mean value of $F_{\alpha i}$; $f_{\alpha i}$ is the fluctuation (with zero mean) of $F_{\alpha i}$ around $\bar{F}_{\alpha i}$.

The mean nodal forces were assigned by the formula:

$$\bar{F}_{\alpha i} = \frac{1}{2}\rho c_{\alpha i} b_i h_i \bar{V}_i^2 \quad (\alpha = x,y;\ i = 3,5,\cdots 17) \tag{9}$$

where z_i, h_i are the height of the center and the tributary height of the i-th element; $\bar{V}_i$ is the mean velocity of the reference wind at the height z_i; c_{xi}, c_{yi} are the alongwind and acrosswind mean force coefficients.

An analytical model of the fluctuating nodal forces was given by (Solari 1985,1994):

$$f_{\alpha i}(t) = f_{\alpha i}^{(u)}(t) + f_{\alpha i}^{(v)}(t) + f_{\alpha i}^{(s)}(t) \quad (\alpha = x,y;\ i = 3,5,\cdots 17) \tag{10}$$

where $f_{\alpha i}^{(u)}$, $f_{\alpha i}^{(v)}$, $f_{\alpha i}^{(s)}$ are the contributions of the longitudinal turbulence (u), of the lateral turbulence (v) and of the vortex shedding (s). They are schematized by multi-dimensional stochastic stationary Gaussian processes and characterized, in the domain of frequency n, by their cross-*psdf* (*cpsdf*) $S_{f\alpha ij}^{(u)}$, $S_{f\alpha ij}^{(v)}$, $S_{f\alpha ij}^{(s)}$. Considering these processes as statistically independent, the *cpsdf* of $f_{\alpha i}$ and $f_{\alpha j}$ becomes:

$$S_{f\alpha ij}(n) = S_{f\alpha ij}^{(u)}(n) + S_{f\alpha ij}^{(v)}(n) + S_{f\alpha ij}^{(s)}(n) \quad (\alpha = x,y;\ i,j = 3,5,\cdots 17) \tag{11}$$

$$S_{f\alpha ij}^{(\varepsilon)}(n) = \sqrt{S_{f\alpha i}^{(\varepsilon)}(n) S_{f\alpha j}^{(\varepsilon)}(n)}\, Coh_{f\alpha ij}^{(\varepsilon)}(n) \quad (\varepsilon = u, v, s) \tag{12}$$

where $S_{f\alpha i}^{(\varepsilon)}$ is the *psdf* of $f_{f\alpha i}^{(\varepsilon)}$; $Coh_{f\alpha ij}^{(\varepsilon)}$ is the coherence function of $f_{\alpha i}^{(\varepsilon)}$, $f_{\alpha j}^{(\varepsilon)}$. Consistently with classical analyses, $S_{fxij}^{(v)}(n) = 0$ and $S_{fxij}^{(s)}(n) = 0$.

The *psdf* of the forces due to the longitudinal turbulence was given by:

$$S_{f\alpha i}^{(u)}(n) = (\rho c_{\alpha i} b_i h_i \bar{V}_i)^2 S_u(z_i; n) \quad (\alpha = x,y;\ i = 3,5,\cdots 17) \tag{13}$$

where S_u is the *psdf* of the longitudinal turbulence (ESDU 1974):

$$\frac{n S_u(z_i; n)}{\sigma_{ui}^2} = \frac{4nL_{ui}/\bar{V}_i}{[1 + 70.8(nL_{ui}/\bar{V}_i)^2]^{5/6}} \quad (i = 3,5,\cdots 17) \tag{14}$$

L_{ui}, $\sigma_{ui} = I_{ui}\bar{V}_i$, I_{ui} are the integral length scale, the *rms* value and the intensity of the longitudinal turbulence at the height z_i, respectively.

The coherence of the forces due to the longitudinal turbulence was determined by the procedure proposed by Solari (1985). The coherence of the alongwind forces depends on the C_{uz} exponential decay factor of the longitudinal turbulence in the vertical direction. The coherence of the acrosswind forces mainly depends on the cross-correlation of pressures on the side faces.

The *psdf* of the acrosswind forces due to the lateral turbulence was set:

$$S_{fyi}^{(v)}(n) = \left(\frac{1}{2}\rho c'_{yi} b_i \bar{V}_i\right)^2 S_v(z_i; n) \quad (i = 3,5,\cdots 17) \tag{15}$$

where c'_{yi} is the prime angular derivative of the mean force coefficient in the y direction; S_v is the *psdf* of the lateral turbulence (ESDU 1974):

$$\frac{n S_v(z_i; n)}{\sigma_{vi}^2} = \frac{4nL_{vi}/\bar{V}_i\,[1 + 755.2(nL_{vi}/\bar{V}_i)^2}{[1 + 283.2(nL_{vi}/\bar{V}_i)^2]^{11/6})} \quad (i = 3,5,\cdots 17) \tag{16}$$

L_{vi}, $\sigma_{vi}=I_{vi}\,\overline{V}_i$, I_{vi} are the integral length scale, the *rms* value and the intensity of the lateral turbulence at the height z_i, respectively.

The coherence of the acrosswind forces due to the lateral turbulence was given by (ESDU 1975):

$$Coh_{f\alpha ij}^{(v)}(n)=\exp\left\{-\frac{2nC_{vz}\,|z_i-z_j|}{\overline{V}_i+\overline{V}_j}\right\}\quad (i,\ j=3,5,\cdots 17) \tag{17}$$

where C_{vz} is the exponential decay factor of the lateral turbulence in the vertical direction.

The *psdf* of the acrosswind forces due to the vortex wake was given by (Solari 1985):

$$S_{fyi}^{(s)}(n)=\left(\frac{1}{2}\rho b_i h_i \overline{V}_i^2 \widetilde{C}_{Li}\right)^2 \frac{\beta_i\,(1-0.64\beta_i^2)n}{(0.964-0.353\beta_i)n_{si}^2}\cdot$$
$$\cdot\frac{1}{[1-(1-0.64\beta_i^2)(n/n_{si})^2]^2+2.56\beta_i^2(1-0.64\beta_i^2)(n/n_{si})^2}\quad (i=3,5,\cdots,17) \tag{18}$$

where $\widetilde{C}_{Li}$ is the *rms* wake lift coefficient, β_i is the spectral bandwidth parameter, $n_{si}=S_i\,\overline{V}_i/b_i$ is the central frequency of the vortex shedding, S is the Strouhal number of the i-th element.

The coherence of the acrosswind forces due to vortex shedding was given by (Vickery and Clark 1972):

$$Coh_{f\alpha ij}^{(J)}(n)=\cos(\alpha_1\Delta_{ij})\exp[-(\Delta_{ij}/\alpha_2)]\quad (i,j=3,5,..17) \tag{19}$$

where $\Delta_{ij}=2\,|z_i\text{-}z_j|/(b_i+b_j)$, $\alpha_1=2/3$, $\alpha_2=3$.

It was finally assumed that $I_{\varepsilon i}=\gamma\, I^*_{\varepsilon i}$, $L_{\varepsilon i}=\delta_\varepsilon L^*_{\varepsilon i}$ (ε=u, v), $C'_{yi}=C'_{yo}$, $C_{vz}=0.9C_{uz}$, $S_i=S_o$, $\beta_i^2=\beta_o^2+2I_{ui}^2$, $\widetilde{C}_{Li}=\widetilde{C}_{Lo}$, $I^*_{\varepsilon i}$, $L^*_{\varepsilon i}$ being the intensity and the integral length scale of the ε=u,v turbulence components of the reference wind. The nondimensional quantities γ, C_{uz}, δ_u, δ_v, C'_{yo}, S_o, β_o, $\widetilde{C}_{Lo}$ are referred to as the spectral parameters.

Mean pressure coefficients in Table 3 and spectral parameters in Table 4 were determined by equating the analytical and measured values of the base reactions through the aerodynamic identification procedure developed by Solari, *et al.* (1996,1997) just for the purpose of this study.

Table 3(a) shows that the mean force coefficients in the alongwind direction are quite homo-

Table 3(a) Alongwind mean force coefficients

$\overline{\alpha}_r(^o)$	c_{3x}	c_{5x}	c_{7x}	c_{9x}	c_{11x}	c_{13x}	c_{15x}	c_{17x}
0	2.671	1.337	1.084	0.949	0.865	0.804	0.749	0.696
12	2.873	1.438	1.139	0.953	0.829	0.736	0.670	0.622
57	1.715	0.859	0.719	0.669	0.644	0.630	0.601	0.558
102	1.435	0.718	0.614	0.593	0.588	0.590	0.569	0.529
135	1.234	0.3618	0.559	0.590	0.624	0.658	0.648	0.602
165	1.815	0.908	0.791	0.788	0.800	0.817	0.795	0.739
192	1.724	0.863	0.742	0.723	0.722	0.727	0.703	0.654
230	2.008	1.005	0.824	0.738	0.687	0.652	0.613	0.570
270	1.139	0.570	0.531	0.584	0.636	0.683	0.678	0.630
305	-0.197	-0.098	-0.010	0.110	0.203	0.281	0.304	0.283
345	2.366	1.185	0.978	0.887	0.834	0.799	0.755	0.702

Table 3(b) Acrosswind mean force coefficients

$\bar{\alpha}_r(^o)$	c_{3y}	c_{5y}	c_{7y}	c_{9y}	c_{11y}	c_{13y}	c_{15y}	c_{17y}
0	-0.659	-0.330	-0.214	-0.097	-0.010	0.061	0.089	0.083
12	-0.469	-0.235	-0.159	-0.087	-0.033	0.011	0.029	0.027
57	-0.420	-0.210	-0.157	-0.114	-0.084	-0.060	-0.047	-0.044
102	-0.469	-0.235	-0.159	-0.087	-0.033	0.011	0.029	0.027
135	-0.329	-0.165	-0.107	-0.048	-0.005	0.030	0.044	0.041
165	0.280	0.140	0.105	0.076	0.056	0.040	0.031	0.029
192	0.420	0.210	0.157	0.114	0.084	0.060	0.046	0.043
230	0.305	0.152	0.106	0.062	0.030	0.005	-0.007	-0.006
270	-0.915	-0.456	-0.318	-0.186	-0.090	-0.015	0.021	0.018
305	0.140	0.070	0.052	0.038	0.028	0.020	0.015	0.014
345	-0.189	-0.095	-0.055	-0.010	0.023	0.050	0.060	0.056

Table 4 Spectral parameters of the aerodynamic model

$\bar{\alpha}_r(^o)$	γ_u	C_{uz}	δ_{lu}	δ_{lv}	C'_{yo}	β_o	S_o	$\tilde{C}_{Lo}$
0	0.88	11.5	1.23	1.38	.468	0.40	0.21	.145
12	0.92	11.5	1.27	2.42	.534	0.40	0.21	.145
57	1.19	11.5	1.23	1.27	.645	0.40	0.16	.123
102	1.11	11.5	1.20	2.19	.556	0.35	0.14	.130
135	1.05	11.5	1.12	2.31	.593	0.50	0.15	.125
165	0.92	11.5	1.44	1.35	.522	0.60	0.17	.130
192	0.99	11.5	1.22	1.12	.415	0.40	0.19	.133
230	0.92	11.5	0.72	1.65	.312	0.20	0.16	.140
270	0.95	11.5	0.75	2.38	.475	0.50	0.15	.147
305	2.43	9.0	0.13	1.69	.400	0.25	0.10	.180
345	0.87	11.5	1.14	1.46	.459	0.45	0.18	.153

geneous with values ranging from 0.55 to 1.00 in the middle and upper part of the tower due to the presence of the surrounding buildings. They are usually higher and scattered in the lower part. When $\bar{\alpha}_r$=305°, the cathedral gives rise to a shielding effect which drastically reduces the alongwind mean force coefficients. With rare exceptions limited to the first orders of the tower, Table 3(b) points out that the acrosswind mean force coefficients are very small whatever the wind direction may be.

Fig. 14 shows some comparisons between the quasi-static psdf of the measured (thin lines) and calculated (thick lines) base overturning moments M_{1x}, M_{1y}. The thick dotted lines indicate the contribution associated with the actions of the longitudinal turbulence. The thick dashed lines correspond to the contributions from the longitudinal and lateral turbulence. The difference between the thick solid lines and the thick dashed lines expresses the contribution of the vortex wake which represents the main loading mechanism in the acrosswind direction.

The aerodynamic model reproduces the experimental measurements with a high degree of precision. It provides a means for easily predicting loads and responses for a broader range of prototype frequencies than is appropriate for experimental measurements. It is immune to resonance effects associated with the mechanical admittance of the base-balance-model system. In addition to the base reactions provided by the force-balance tests, it furnishes consistent estimates of the distributed forces applied by the wind on the tower. Except for $\bar{\alpha}_r$=305° and for β_o coefficients,

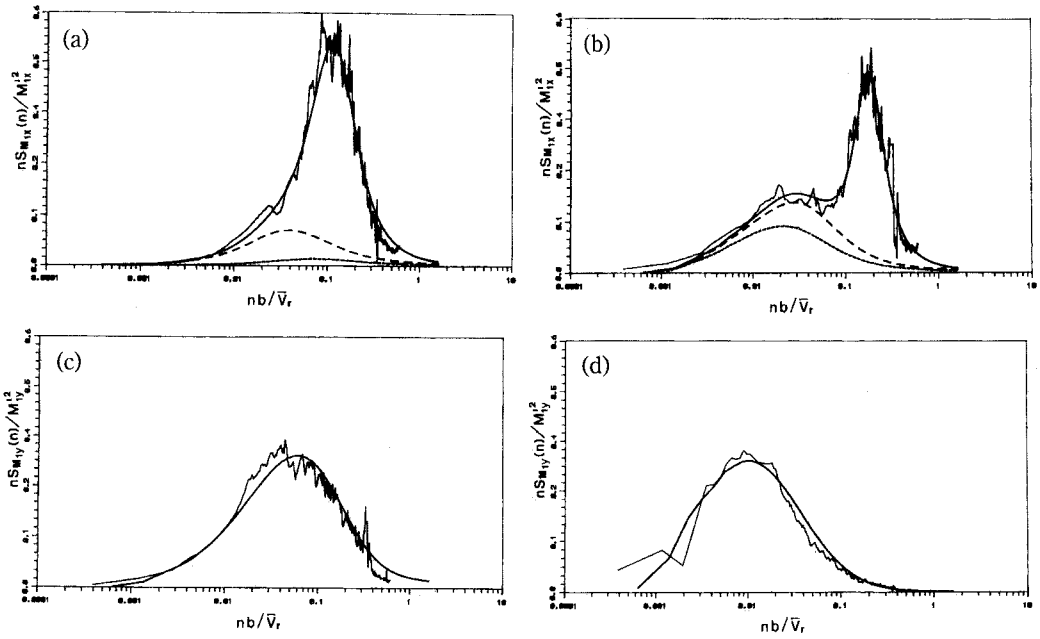

Fig. 14 *Psdf* of the quasi-static components of the measured and calculated fluctuating base overturning moment: (a) M_{1x} for $\bar{\alpha}_r$=0° (b) M_{1x} for $\bar{\alpha}_r$=305° (c) M_{1y} for $\bar{\alpha}_r$=0° (d) M_{1y} for $\bar{\alpha}_r$=305°.

spectral parameters assume homogeneous values generally corresponding to those provided by the literature. The dependence of these values on the wind direction is clearly due to the disturbing effects of the buildings surrounding the tower.

For $\bar{\alpha}_r$=305°, the presence of the cathedral immediately upstream of the tower gives rise to a phenomenon of the wake buffeting type, whose spectral content is definitely different from that of the forces associated with other wind directions. In this situation, the intensity of the alongwind fluctuating forces significantly exceeds that of the mean static forces.

The β_o spectral parameters defining the bandwidth of the vortex shedding assume higher values than those reported in the literature with reference to usual cylindrical bodies (Vickery and Clark 1972, ESDU 1990). It seems reasonable to expect that the loggias make the wake chaotic to the extent of spreading its harmonic content well outside the traditional bandwidth.

7. Dynamic response

The probabilistic study of the wind-excited response of the tower was based on two sequential steps. In the first step, the parametric analysis of the dynamic response was carried out by varying the reference velocity $\bar{V}_r$ and the reference direction $\bar{\alpha}_r$. In the second step, combining the results of this study with the probability distributions of $\bar{V}_r$, $\bar{\alpha}_r$, the structural effects were expressed as functions of the mean return period. A full discussion concerning the equivalent static forces and the sensitivity of the response to selected mechanical parameters is presented by Solari, *et al.* (1997).

7.1. Parametric analysis of the dynamic response

The parametric analysis of the wind excited response of the Tower of Pisa was carried out in the elastic linear field by the computer program WL3D (Solari 1986). The program input in-

cludes characteristics of the oncoming wind, the natural frequencies, normal modes and damping coefficients of the structure and the aerodynamic parameters described by the preceding section. The output consists of the statistical averages (Davenport 1964) of the alongwind and acrosswind components, E_x, E_y, of the selected structural effects E (internal forces, generalized displacements, accelerations, ..):

$$E_{\alpha max} = \bar{E}_\alpha + g_{e\alpha}\sigma_{e\alpha} \quad (\alpha = x, y) \tag{19}$$

$$E_{\alpha min} = \bar{E}_\alpha - g_{e\alpha}\sigma_{e\alpha} \quad (\alpha = x, y) \tag{20}$$

$$\sigma_{e\alpha}^2 = \int_0^\infty S_{e\alpha}(n)dn \quad (\alpha = x, y) \tag{21}$$

$$g_{e\alpha} = \sqrt{2\ln(\nu_{e\alpha}T)} + \frac{0.5772}{\sqrt{2\ln(\nu_{e\alpha}T)}} \quad (\alpha = x, y) \tag{22}$$

$$\nu_{e\alpha}^2 = \frac{\int_0^\infty n^2 S_{e\alpha}(n)dn}{\int_0^\infty S_{e\alpha}(n)dn} \quad (\alpha = x, y) \tag{23}$$

where $\bar{E}_\alpha$ is the mean value of E_α; $E_{\alpha max}$, $E_{\alpha min}$ are the mean maximum and minimum values of E_α; $\sigma_{e\alpha}$, $S_{e\alpha}$, $\nu_{e\alpha}$, $g_{e\alpha}$ are the *rms* value, the *psdf*, the expected frequency and the peak factor of $e_\alpha = E_\alpha - \bar{E}_\alpha$; T=10 minutes.

Consider the resultant effect:

$$E = \sqrt{E_x^2 + E_y^2} \tag{24}$$

Let the probability that a given quantity exceeds its mean maximum value be defined as small.

If E_x, E_y are non-correlated random processes, a small probability exists that E goes out of the solid line ellipse in Fig. 15. In the opposite case in which E_x, E_y are random processes positively or negatively perfectly correlated, E lies, with a small probability of going outside, on the diagonals BD or AC of the rectangle ABCD. In every case the probability is small that E goes out of the rectangular threshold ABCD.

Assuming alongwind and acrosswind forces as non-correlated, E_x, E_y are non-correlated and E lies inside of the solid line ellipse in Fig. 15, with a small exceedance probability. In fact, this is not conservative, since any exception to the theoretical hypothesis makes the probability that E goes out of the ellipse significant. Therefore, introducing a criterion which generalizes the method proposed by Simiu and Scanlan (1996), it was assumed that E lies inside of the polygon joining the points P_1, P_2, .. P_{12}, with a small probability of going out of this threshold. For the purpose of this study, $\eta = 0.3$, $\gamma = 0.8$.

The mean maximum value E_{max} of the resultant effect E is the length of the vector joining the origin of the E_x, E_y plane with the farthest point of the polygon P_1, P_2, .. P_{12}. The mean maximum component of E in a given direction, in particular the x' axis of maximum slope or the y' orthogonal axis, is the length of the projection of this vector in that direction.

The dynamic response of the tower was calculated for the 6 velocities $\bar{V}_r$=10,15,20,25,30,35 m/s

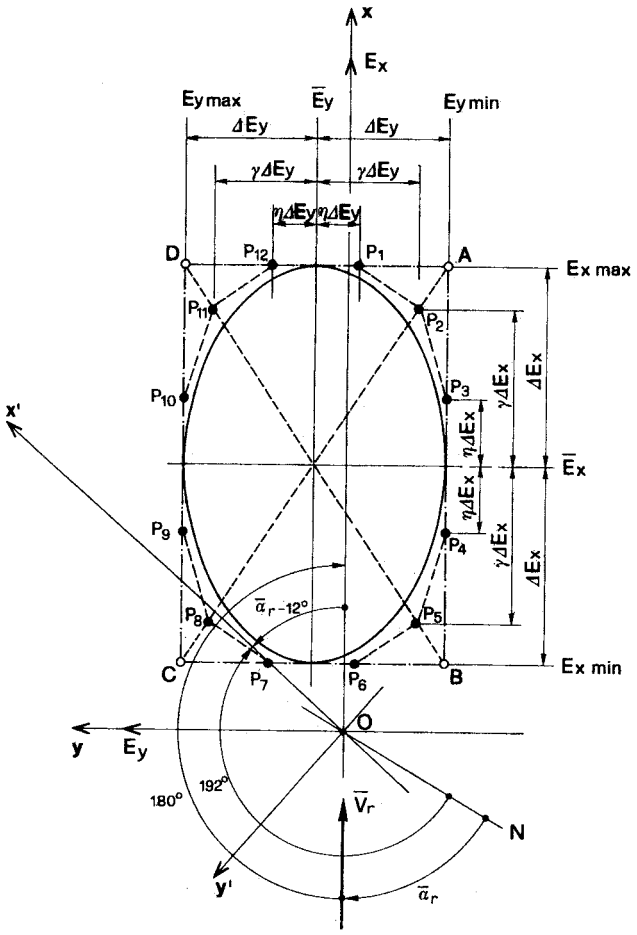

Fig. 15 Resultant effects and component effects in the plain of maximum slope and in its orthogonal plane

and the 11 directions $\overline{\alpha_r}$=0,12,57,102,135,165,192,230,270,305,345 degrees. In all, 66 analyses were carried out. Fig. 16 shows the polar diagrams of the mean maximum values of the x, y components of the base overturning moment, M_{1x}, M_{1y}, of their resultant value M_1, of its component in the plane of maximum slope $M_{1/}$. The points along the innermost contour correspond, for the different wind directions, to V_r=10 m/s; other contours correspond to V_r=15,20,25,30,35 m/s.

Except for $\overline{\alpha_r}$=305°, where the cathedral shielding effect reduces the alongwind forces, the maximum alongwind response decidedly exceeds the maximum acrosswind response by a factor of the order of 3 for $\overline{V_r}$=10 m/s, of 2 for $\overline{V_r}$=35 m/s. The maximum resultant effects are therefore almost coincident with the maximum alongwind effects. As far as concerns the maximum effects in the plane of the maximum slope, they are the highest and coincide with the maximum alongwind effects when wind is directed from the north; they are the lowest and practically negligible when wind is directed from the south; they assume intermediate values, very like the maximum acrosswind effects, when wind is directed from the east or from the west.

7.2. Probabilistic analysis of the structural response

Using relationships of the type shown in Fig. 16, the data base $\overline{V_r}$, $\overline{\alpha_r}$ may be transformed into

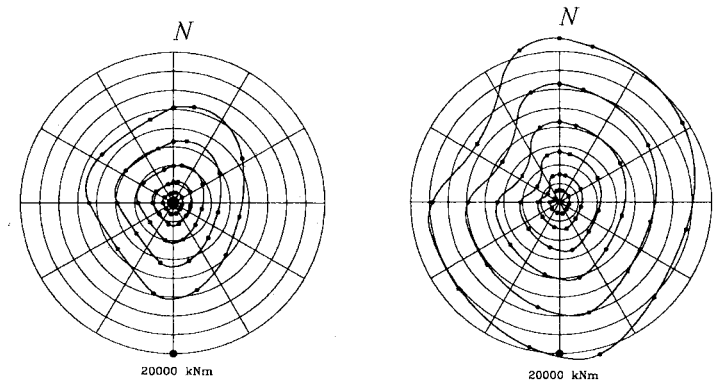

Fig. 16 Polar diagrams of: (a) M_{1x}; (b) M_{1y}; (c) M_1; (d) $M_{1/}$

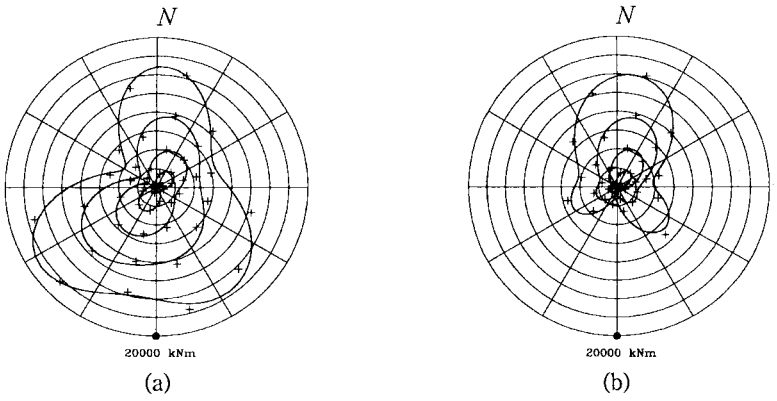

Fig. 17 Joint distributions of: (a) M_1, $\overline{\alpha}_R$; (b) $M_{1/}$, $\overline{\alpha}_R$

new data bases, E, $\overline{\alpha}_r$, E being a generic effect. The probabilistic analysis of these effects was carried out adopting the methods applied to wind velocity in Sections 3.1 and 3.2.

Fig. 17 shows the polar joint distributions of E, $\overline{\alpha}_r$ (E=M_1, $M_{1/}$): each point along the innermost contour represents the effect exceeded on average 1% of the time, due to the wind from a 30°sector centered on that direction; other contours correspond to probability levels of 0.1%,

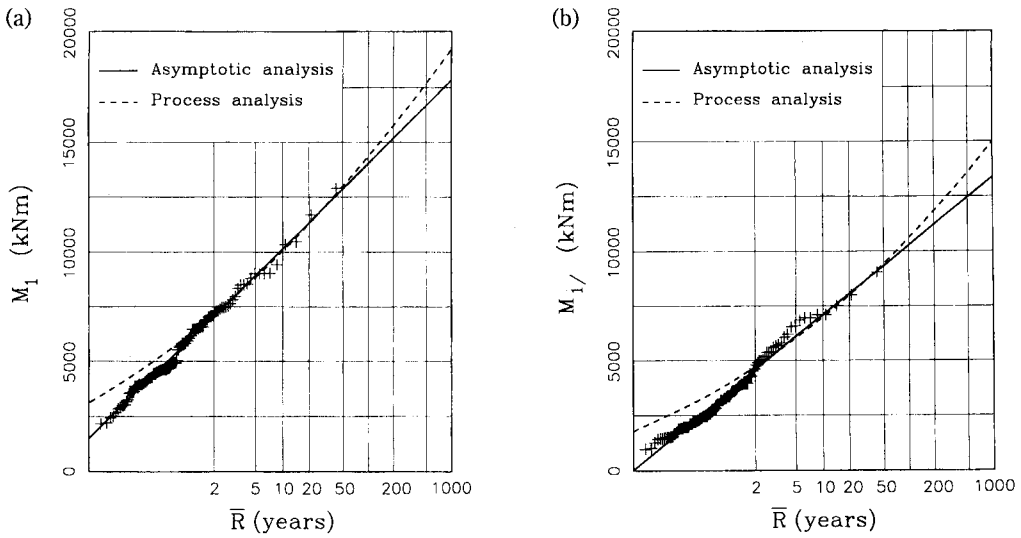

Fig. 18 Distribution of the yearly maximum value of: (a) M_1; (b) $M_{1/}$

0.01%, 0.001%, 0.0001%. The maximum values of the resultant effects are mainly caused by the winds directed from the north, south-east and south-west; this is due to the fact that the maximum values of the reference velocity and, for the same velocity, the maximum values of the resultant effects simultaneously occur from these directions. The maximum effects in the plane of maximum slope are mainly due to the winds directed from the north. The shielding role of the cathedral avoids the occurrence of relevant effects when the wind is directed from the north-west.

Fig. 18 shows the distributions of the yearly maximum effects; the solid and dashed lines correspond to the asymptotic and to the process analysis. They provide very similar results for average return periods; for high $\bar{R}$ values, the asymptotic analysis is less conservative than the process analysis. This was explained by noting that the dynamic response is approximately proportional to the squared wind velocity; the k exponents of the Weibull functions of the structural effects are therefore almost half of the k velocity values (Solari 1996a); as such, they are less than one and the trend of the process analysis is opposite to that found for the wind velocity (Lagomarsino, *et al.* 1992).

The comparison between Fig. 18(a) and Fig. 18(b) shows that the ratio between the maximum effects in the plane of maximum slope and those provided by the nondirectional study lie in the range from 0.70 to 0.75 for $\bar{R}$=10 and from 0.80 to 0.85 for $\bar{R}$=1000 years.

Above all it is apparent that the base overturning moments $M_{1/}$ caused by wind in the plane of maximum slope are very small in comparison with the M_o=326,171 kNm overturning moment due to the weight eccentricity. In particular, for $\bar{R}$=1000 years, $M_{1/}$ is less than 5% of M_o.

8. Conclusions

This paper describes wind investigations which were conducted for the Committee of Consolidation and Restoration Interventions on the Leaning Tower of Pisa, as part of an overall evaluation of its behaviour.

The analyses were carried out partly using well-known methods consistent with the state-of-the-art, partly introducing new approaches (the aerodynamic identification criterion; the evaluation of the maximum resultant effects and of their maximum components in the plane of max-

imum slope) aimed at attaining levels of precision adequate for the importance of this problem. Every time it was possible, the analyses were repeated adopting different procedures (probabilistic evaluations, force-balance wind-tunnel tests), or varying the input parameters to ascertain the robustness of the solutions with reference to data uncertainties (Reynolds number, free and forced vibration analyses).

Among several interesting results, the existence of two distinct groups of structural modes should be noted. The first two pairs are classic soil-structure interaction mode shapes producing energy dissipation mainly in the soil. The upper modes are characterized by displacements and damping properties associated with the masonry part of the structure.

The joint application of high-frequency force-balance wind-tunnel tests and analytical identification procedures provides a clear picture of the aerodynamic behaviour of the Leaning Tower of Pisa. In the case of north-west winds, the presence of the cathedral immediately upstream of the tower gives rise to a wake buffeting phenomenon, where fluctuating alongwind and acrosswind forces have similar intensities, while mean static actions are very small. In all other cases the alongwind forces, of the classic type, definitely prevail over the acrosswind actions.

As a consequence, the maximum effects in the plane of the maximum slope almost coincide with the maximum alongwind effects when wind is directed from the north. The base overturning moments in this direction are 15%-30% less than those furnished by the nondirectional study and, most significantly, less than 5% of the base overturning moment due to the weight eccentricity.

If necessary, all these results may be further improved. The knowledge of the wind field at the site could be confirmed or refined using anemometer records recently acquired at the top of the tower. The measurement of the structural frequencies, modes and damping coefficients should not involve relevant modifications of the structural response; however, it should allow the validation or the calibration of the models and of their estimates. Carrying out full-scale experiments to obtain simultaneosus values of wind velocities and structural stresses and displacements might represent an effective check of the wind-tunnel tests and of the theoretical methods applied for deriving the aerodynamic actions. When these measurements will be available, the procedure developed herein will allow a simple and rapid review of the models and of the results.

Acknowledgements

The Authors are grateful to Professor Jamiolkowski, to Professor Macchi and to all members of the Committee of Consolidation and Restoration Interventions on the Tower of Pisa for their encouragement and the opinions expressed for the work carried out. They also thank all those who collaborated to make this study possible and, in particular, the Consorzio Progetto Torre di Pisa and Ing. Heineger who provided the basic material, Dr. Piccardo of the Department of Structural and Geotechnical Engineering of Genova University who collaborated to statistical analyses, Professor Buresti of the Department of Aerospace Engineering of Pisa University who gave his advice and participated in the review of wind-tunnel tests, the staff of the Wind Engineering Department at DMI for their assistance in running the wind tunnel tests and for their hospitality, Clemson University for constructing the proximity model, Professors Castiglioni, Faccioli, Grandori and Perotti of the Department of Structural Engineering of Milan Polytechnic for the kind cooperation in the implementation of the structural model.

References

Associazione Geotecnica Italiana (1993), "The Leaning Tower of Pisa. Present situation", *Proc. 10th Eur.*

Conf. on Soil Mechanics and Foundation Engineering, Florence, Italy.
Ballio, G., Lagomarsino, S., Piccardo, G. and Solari, G. (1993), "A first step towards a map of Italian extreme winds. Part 1: General principles and analysis methodology", *Costruzioni Metalliche,* **3**, 147-172.
Burland, J.B. and Potts, D.M. (1994), "Development and application of a numerical model for the Leaning Tower of Pisa", *Proc. Int. Symp. on Pre-failure Deformation Characteristics of Geo-materials*, IS-Hokkaido, Japan.
Davenport, A.G. (1964), "Note on the distribution of the largest value of a random function with application to gust loading", *Proc. Instn. Civ. Engng.,* **24**, 187-196.
Davenport, A.G. (1968), "The dependence of wind loads on meteorological parameters", *Proc. Int. Conf. on Wind Effects on Buildings and Structures*, Ottawa, Canada, **1**, 19-82.
Engineering Sciences Data Unit (1974), "Characteristics of atmospheric turbulence near the ground. Part II: Single point data for strong winds (neutral atmosphere)", *ESDU 74031*, London, U.K.
Engineering Sciences Data Unit (1975), "Characteristics of atmospheric turbulence near the ground. Part III: Variations in space and time for strong winds (neutral atmosphere)", *ESDU 75001*, London, U.K.
Engineering Sciences Data Unit (1990), "Circular-cylindrical structures: dynamic response to vortex shedding. Pt. 1: Calculation procedures and derivation", *ESDU 85038*, London, U.K.
Engineering Sciences Data Unit (1992), "Computer program for wind speeds and turbulence properties: flat or hill sites in terrain with roughness changes", *ESDU 92032*, London, U.K.
Faccioli, E. and Grandori, G. (1994), "Seismic verification of the Tower of Pisa", Final Report, Committee of Consolidation and Restoration Interventions on the Tower of Pisa, (in Italian).
Gomes, L. and Vickery, B.J. (1977), "On the prediction of extreme wind speeds from parent distribution", *J. Ind. Aerod.,* **2**, 21-36.
Gumbel, E.J. (1958). Statistics of extremes, Columbia University, New York, N.Y.
Hoaglin, D.C., Mostaller, F., and Tukey, J.W. (1983). Understanding robust and exploratory data analysis, John Wiley, New York, N.Y.
Lagomarsino, S., Piccardo, G. and Solari, G. (1992), "Statistical analysis of high return period wind speeds", *J. Wind Engng. Ind. Aerod.,* **41**, 485-496.
Simiu, E., and Scanlan, R.H. (1996). Wind effects on structures, John Wiley, New York, N.Y.
Solari, G. and Stura, D. (1979), "Effects of soil-structure interaction on the dynamic along-wind response of structures", *Proc. Int. Conf. on Environmental Forces on Engineering Structures*, London, U.K., 75-89.
Solari, G. (1985), "Mathematical model to predict 3-D wind loading on buildings", *J. Engng. Mech., ASCE*, **111**, 254-276.
Solari, G. (1986), "3-D response of buildings to wind action", *J. Wind Engng. Ind. Aerod.,* **23**, 379-393.
Solari, G. (1994), "Gust-excited vibrations", in *Wind-excited vibrations of structures*, Sockel, H., Editor, Springer-Verlag, Wien, 195-291.
Solari, G. (1996a), "Wind speed statistics", in *Modelling of the atmospheric flow fields*, Lalas, D.P. and Ratto, C.F., Editors, World Scientific, Singapore, 637-657.
Solari, G. (1996b), "Statistical analysis of extreme wind speeds", in *Modelling of the atmospheric flow fields*, Lalas, D.P. and Ratto, C.F., Editors, World Scientific, Singapore, 659-678.
Solari, G., Pagnini, L.C., and Piccardo, G. (1996), "High-frequency force balance wind tunnel tests and aerodynamic identification of structures", Istituto di Scienza delle Costruzioni, University of Genova, Series II, 2.
Solari, G., Pagnini, L.C. and Piccardo, G. (1997a), "A numerical algorithm for the aerodynamic identification of structures", *J. Wind Engng. Ind. Aerod.*, in press.
Solari, G., Reinhold, T.A. and Livesey, F. (1997b), "The actions and effects of wind on the Leaning Tower of Pisa", Department of Structural and Geotechnical Engineering, University of Genova, Series II, 1.
Vickery, B.J. and Clark, A.W. (1972), "Lift or across-wind response of tapered stacks", *J. Struct. Div., ASCE*, **98**, 1-20.
Weibull, W. (1951), "A statistical distribution function of wide applicability", *J. Appl. Mech.,* **18**, 293-297.
Zilitinkevich, S.S. (1989), "Velocity profiles, the resistance law and the dissipation rate of mean flow kinetic energy in a neutrally and stably stratified planetary boundary layer", *Bound. Lay. Meteorol.,* **16**, 367-386.